Methanol Operation in Heavy-Duty DICI Dual-Fuel Engines
Investigating Charge Cooling Effects Using Engine Combustion Network Spray D Data

Zoumpourlos, Konstantinos; Geertsma, Rinze; Van De Ketterij, Robert; Coraddu, Andrea

DOI
10.1115/1.4067862

Publication date
2025

Document Version
Final published version

Published in
Journal of Engineering for Gas Turbines and Power

Citation (APA)
Zoumpourlos, K., Geertsma, R., Van De Ketterij, R., & Coraddu, A. (2025). Methanol Operation in Heavy-Duty DICI Dual-Fuel Engines: Investigating Charge Cooling Effects Using Engine Combustion Network Spray D Data. *Journal of Engineering for Gas Turbines and Power*, *147*(10), Article 101007. https://doi.org/10.1115/1.4067862

ASME Journal of Engineering for Gas Turbines and Power
Online journal at:
https://asmedigitalcollection.asme.org/gasturbinespower

Methanol Operation in Heavy-Duty DICI Dual-Fuel Engines: Investigating Charge Cooling Effects Using Engine Combustion Network Spray D Data

Konstantinos Zoumpourlos[1]
Sustainable Drive & Energy Systems,
Faculty of Mechanical Engineering,
Department Maritime & Transport Technology,
Delft University of Technology,
Delft 2628 CD, The Netherlands
e-mail: k.zoumpourlos@tudelft.nl

Rinze Geertsma
Faculty of Military Sciences,
Netherlands Defence Academy,
Den Helder 4811 XC, The Netherlands
e-mail: rd.geertsma@mindef.nl

Robert van de Ketterij
Faculty of Military Sciences,
Netherlands Defence Academy,
Den Helder 4811 XC, The Netherlands
e-mail: rg.vd.ketterij@mindef.nl

Andrea Coraddu
Sustainable Drive & Energy Systems,
Faculty of Mechanical Engineering,
Department Maritime and Transport Technology,
Delft University of Technology,
Delft 2628 CD, The Netherlands
e-mail: a.coraddu@tudelft.nl

Methanol is a promising alternative fuel, which can assist in reducing emissions in heavy-duty (HD) dual-fuel (DF) compression ignition (CI) engines. In medium and large bore marine engines, DF operation is achieved through either direct injection (DI) or port fuel injection (PFI) of methanol with diesel acting as a DI pilot fuel for ignition. However, the injection of methanol presents a significant challenge due to its high latent heat of vaporization and decreased lower heating value (LHV) compared to diesel. Therefore, for the same energy content operation, methanol requires around eight times the amount of heat to evaporate completely in comparison to diesel, which results in lower in-cylinder temperatures. This charge cooling effect leads to a strong negative temperature gradient influencing ignition and flame propagation. This paper aims to quantify the cooling effect of methanol in a heavy-duty dual-fuel direct injection compression ignition (DICI) engine environment. The presented methodology uses computational fluid dynamics (CFD) simulations to model methanol sprays with validation originating from the engine combustion network (ECN) Spray D experimental data. The CFD models operate within the Lagrangian–Eulerian framework in CONVERGE-CFD using the Reynolds Averaged Navier Stokes (RANS) turbulence modeling. Compared to diesel, injecting methanol with the same energy content exhibited up to 100 K more decreased temperature within the mixture. Consequently, this cooled mixture may pose challenges to combustion stability due to the intense temperature gradients. Nonetheless, lower mixture temperature decreases NO_x emissions, which can prove beneficial for high methanol energy fractions in dual-fuel DICI engines. [DOI: 10.1115/1.4067862]

Keywords: methanol, computational fluid dynamics, spray modeling, alternative fuels

1 Introduction

In the heavy-duty (HD) automotive and marine sector, power and propulsion is mainly realized by diesel compression ignition (CI) internal combustion engines (ICEs), which cause local (NO_x, SO_x, unburned hydrocarbons, and soot) and global CO_2 emissions [1–3]. Despite recent advances in the use of alternative energy sources, ICEs will remain at the forefront of power generation due to their power density, robustness, and cost advantages [4,5]. To mitigate the combustion emissions issue, alternative fuels produced from biomass or captured CO_2 can assist in decarbonizing ICEs [6,7]. Among the candidate alternative fuels, methanol is a promising contender owing to its advantageous properties (e.g., high burning velocity, low combustion temperature), scalable production, and lower hazardous emissions, such as NO_x, SO_x, and soot, compared to diesel [8,9]. Contrary to ammonia and hydrogen, methanol is liquid at atmospheric conditions, which simplifies transportation and storage, while having adequate energy density [10]. For these reasons, methanol is considered the most cost-effective sustainable fuel option for the transportation sector [11].

Methanol combustion in CI HD engines is commonly accomplished by either dual-fuel (DF) operation using a pilot fuel for ignition or the addition of ignition improvers [8,12]. In DF engines, methanol is premixed with the air, through either port fuel injection (PFI) or direct injection (DI), creating a low reactivity mixture. This premixed charge has the main energy content and is ignited by a high reactivity fuel, like diesel, initiating the flame propagation [13,14]. However, increasing diesel substitution in DF engines is limited due to methanol's high latent heat of vaporization and high auto-ignition temperature. Methanol's phase transition draws about eight times more energy from the in-cylinder air compared to diesel. Eventually, the air–fuel mixture will have a significantly decreased temperature prior to combustion initiation [15].

Previous studies on HD methanol-diesel engines have mainly focused on combustion performance and emissions [16–19]. The reported conclusions in these studies implicitly indicated the strong

The ICE Forward Conference. The Westin Riverwalk. ICEF2024.
[1]Corresponding author.
Manuscript received January 17, 2025; final manuscript received January 29, 2025; published online March 18, 2025. Editor: Jerzy T. Sawicki.

impact of the methanol cooling effect on engine stability and NO_x emissions. Using an optical HD engine, Matamis et al. [19] demonstrated that the cooling effect impedes flame propagation while increasing the ignition delay. Moreover, other experimental studies suggested intake air heating as a way to maintain combustion stability [16,20], especially under low load conditions [17]. Using PFI of methanol, Dierickx et al. [20] stated that the exacerbated cooling intensity even led to the condensation of methanol in the intake manifold. Despite this, lower NO_x emissions than in diesel operation were observed due to lower combustion temperature [16–18,20].

Concerning previous methanol spray-dedicated studies, Wang et al. [21] experimentally compared methanol with diesel sprays in CI engine conditions. Their study demonstrated that at moderate ambient temperatures (600 K) and increased ambient pressures (ranging from 20 to 40 bar), methanol evaporates faster due to its lower boiling point. Their experiments highlighted many similarities in methanol's macroscopic spray structure with diesel. Furthermore, Karimkashi et al. [14] conducted a large eddy simulation study on DF ignition of methanol–air mixtures with n-dodecane acting as pilot fuel. Their simulated conditions showcased nonrobust ignition of the methanol–air mixture and increased ignition delay, which could be attributed to the cooling effect of methanol. In addition, Kaario et al. [22] used engine combustion network (ECN) reacting Spray A data to validate their large eddy simulation framework using n-dodecane under light-duty automotive injection quantities. Subsequently, the validated model was converted for methanol injection using a set of increased ambient temperatures to facilitate ignition. Compared to n-dodecane, the authors reported increased flame liftoff length under lower ambient temperatures. This increase is directly coupled to the reduced mixture temperature, which stems from the augmented latent heat.

While previous research has investigated igniting diesel-methanol sprays with a focus on ignition delay and flame liftoff length [14,22], a significant gap of knowledge exists on the charge cooling during the mixture formation process prior to combustion. To sufficiently understand methanol's impact on mixture formation, predictive computational fluid dynamics (CFD) models can assess the spray behavior under CI engine conditions. This paper aims to study the spray formation, evaporation, and mixing of methanol in a direct injection compression ignition (DICI) engine environment in the context of HD-DF engines. The novelty of this study constitutes of the quantification of the mixture cooling effect originating from methanol injection in comparison to diesel. For the present analysis, CFD modeling was used utilizing the Lagrangian–Eulerian (LE) coupling method to reproduce the multiphase flow phenomena. The model was developed using CONVERGE-CFD [23] following a Reynolds-Averaged Navier Stokes (RANS) turbulence modeling approach in a constant volume chamber.

To validate our models, we used nonreacting data from the n-dodecane ECN Spray D experiments, which are representative of large-nozzle HD injection quantities. Consequently, the validated model was converted for methanol simulation to facilitate near Top-dead-center (TDC) DI typical of DF engines. In the converted model, methanol was implemented through a set of varied properties and altered mass diffusivity constants used for evaporation modeling. The methanol spray model was used for different cases, which represented equal quantity and equal energy injections as the baseline diesel model. To assess the mixture cooling effect, these methanol models were compared with diesel based on their liquid length, the evaporated mass fraction, and the mixture temperature distributions. The results demonstrated an excessive decrease in mixture temperature for the methanol cases. These findings indicate that methanol injection will eventually create cold spots in the cylinder, which impede flame propagation and influence combustion stability, confirming the experimental observations in HD-DF engines.

2 Background

Methanol exhibits a significantly increased latent heat of vaporization, which is four times higher compared to diesel (Table 1). Considering also the reduced lower heating value, approximately eight times extra thermal energy is required for complete evaporation of methanol for the same energy content compared to diesel [25]. Therefore, the extra heat required for the mixture formation leads to lower in-cylinder temperature highlighting an intensive charge cooling effect [15]. Subsequently, methanol combusts differently than diesel, posing long ignition delay and local flame quenching originating from lower mixture temperature [19]. This phenomenon causes increased cycle-to-cycle variability and unstable operation over the working range of methanol engines.

Table 1 Fuel properties [24]

Property	Diesel	Methanol
Lower heating value (LHV) (MJ/kg)	42.7	20.1
Density (at STP) (kg/m^3)	840	790
Heat of vaporization (at 1 bar) (kJ/kg)	250	1089
Boiling point (at 1 bar) (°)	180–360	65
Surface tension (at 20 deg) (mN/m)	27	23
Dynamic viscosity (at 20 deg) (mPa · s)	2.1–2.52	0.57
Cetane number	38–53	<5
Octane number	15–25	109

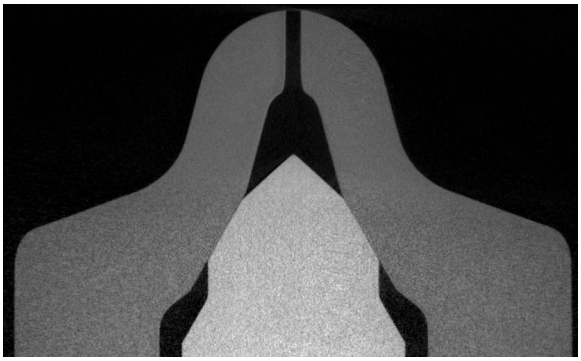

Fig. 1 Spray D X-ray scan provided by Ref. [26]

2.1 Experimental Background. This study used the ECN Spray D to validate our computational models [26]. The Spray D is a Bosch single-hole injector characterized by a convergent channel to minimize cavitation (see Fig. 1). The nozzle diameter is 0.186 mm, making it suitable for HD-DI conditions with large injection quantities. The Spray D experiments were conducted in a constant volume chamber under various ambient conditions reminiscent of CI diesel engines using n-dodecane as a fuel. The ambient conditions were characterized by altered oxygen concentrations ranging from nonreacting to reacting conditions. Since we are investigating the mixture formation phenomena of methanol, we focus on the nonreacting condition with 0% oxygen. Table 2 summarizes the nonreacting Spray D conditions used in our study. Lately, the ECN

Table 2 ECN Spray D nonreacting conditions

Item	Value
Test fuel	N-dodecane
Ambient pressure	60 bar
Ambient temperature	900 K
Fuel temperature	363 K
Injection pressure	150 Mpa
Injection quantity	228 cc/min
Injection duration	4.5 ms
Nozzle diameter	0.186 mm
Ambient gas composition	$O_2 = 0\%$, $N_2 = 89.71\%$, $CO_2 = 6.52\%$, $H_2O = 3.77\%$

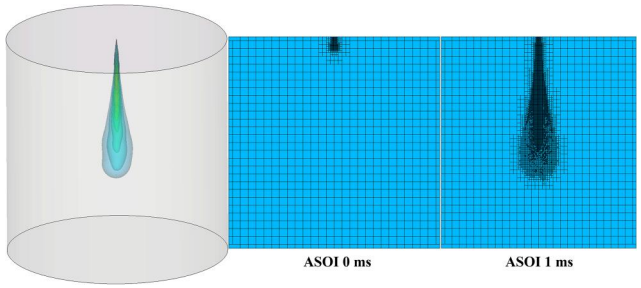

Fig. 2 Simulation control volume and mesh grid at different simulation times

has conducted dedicated methanol spray experiments using a multihole gasoline DI-style injector [27]. Although the experiments use methanol as a fuel, they could not be utilized for validation purposes here, as our focus is HD and marine applications.

3 Computational Methodology

In this study, we used the CONVERGE v3.0 CFD software [23,28] to solve the compressible conservation equations of mass, momentum, and energy. To model turbulence, a RANS approach was followed using the RNG $k-\epsilon$ model [29]. The conservation equations were solved using the density-based solver [30] along with the Pressure Implicit with Splitting of Operators algorithm [31]. The numerical scheme is first-order accurate in time and second order in space. Furthermore, the Courant-Friedrichs-Lewy criterion [30,32] was used to determine the time-step of the simulations. The thermodynamic properties of air, n-dodecane, and methanol were modeled based on the Redlich–Kwong equation of state [33].

3.1 Computational Domain and Mesh Grid. For the computational domain, we created a cylindrical geometry to conduct the numerical computations (Fig. 2) with a 54 mm radius and 108 mm height. The dimensions of the geometry were chosen accordingly with similar ECN spray literature [34,35]. All the cylinder boundary conditions were assigned as wall-type Dirichlet for the temperature and Neumann for the turbulent kinetic energy. The computational domain was discretized with a base cell size of 4 mm with additional manual and automatic refinements in the spray region. The spray cone region was treated with fixed embedding mesh refinement to increase resolution near the nozzle exit (Fig. 2). Moreover, finer mesh resolution was applied using Adaptive Mesh Refinement (AMR) based on velocity and species gradients. The max embedding level was set as 4 leading to a minimum cell size of 0.25 mm. The minimum cell size was selected as the most adequate in terms of computational cost and numerical accuracy [28]. Lastly, the subgrid criterion was set as 0.1 m/s for the velocity refinement and 0.001 fuel mass fraction for the species refinement.

3.2 Spray Model. For the multiphase flow modeling, we used a Lagrangian–Eulerian (LE) coupling approach, which treats the liquid droplets as particles and the gas with Eulerian representation. A suite of phenomenological spray models was applied to the particles to resolve subgrid physical phenomena. Moreover, the computational particles were injected using the Reitz and Diwakar [36] "blob" model. These particles interact with the ambient medium and undergo breakup due to flow instabilities. To model breakup, we used the Kelvin Helmholtz–Rayleigh Taylor (KH-RT) model, which is based on fluid phenomena occurring during atomization and droplet breakup. Initially, primary breakup occurs under Kelvin–Helmholtz hydrodynamic instabilities due to unstable shear waves acting on the interface of the particles and the air [36,37]. Similarly, the aerodynamic drag forces acting on the particles cause the secondary breakup under Rayleigh–Taylor instabilities [36,37].

In the KH model, after breakup occurred, the resulting child droplet radius r_c is established as follows [37]:

$$r_c = B_0 \Lambda_{KH} \tag{1}$$

where Λ_{KH} is the wavelength of the fastest growing wave, and B_0 is the KH model size constant. The parent parcel radius r_p is estimated according to the following expression:

$$\frac{dr_p}{dt} = -\frac{(r_p - r_c)}{\tau_{KH}} \tag{2}$$

where the breakup time τ_{KH} is calculated by

$$\tau_{KH} = \frac{3.726 B_1 r_p}{\Lambda_{KH}\Omega_{KH}} \tag{3}$$

where B_1 is the breakup time constant, and Ω_{KH} is the growth rate of the Λ_{KH} wavelength.

In the RT model, breakup occurs when the droplets decelerate due to unstable waves normal to the spray tip. Hence, the RT instabilities also represent growing waves, which are dictated by the fastest wavelengths [37]. Similarly with the KH model size constant in Eq. (1), the RT model size constant C_{RT} determines the instability wave sizes. Subsequently, breakup occurs when the wavelength scale ($C_{RT}\Lambda_{RT}$) is smaller than the parent droplet diameter while the RT waves grow on the droplet surface for a sufficient time (greater than the breakup time). The RT breakup time τ_{RT} is computed by the following expression:

$$\tau_{RT} = \frac{C_\tau}{\Omega_{RT}} \tag{4}$$

where C_τ is the RT breakup time constant, and Ω_{RT} is the fastest wave growth rate. The resulting child droplet radius r_c is calculated by the following expression:

$$r_c = \frac{C_{RT}\Lambda_{RT}}{2} \tag{5}$$

Particle interactions were modeled by the no time counter algorithm [38], estimating the collisions between droplets. The model of Postand Abraham [39] was used to predict the postcollision outcome, including bouncing, stretching, reflective separation, and coalescence. Furthermore, the particles were coupled to the ambient medium by aerodynamic drag forces and turbulent flow phenomena. The drag force was modeled using a dynamic drag model with altering drag coefficient according to the flow conditions [40]. The particle distortion was considered by Taylor analogy breakup model calculations to ensure a consistent estimation of the drag coefficient. Turbulence effects on the particles were established through a turbulent dispersion model by O'Rourke [41]. Lastly, for evaporation modeling, the Frossling correlation was applied assuming uniform temperature distribution within each particle [42]. The summary of the adopted numerical models is shown in Table 3.

Table 3 Numerical models

Physical phenomena	Numerical models
Fluid flow	Navier stokes, density-based solver [30]
Turbulence	RNG $k-\epsilon$ model [29]
Droplet injection	Blob model [36]
Liquid breakup	KH-RT model [37]
Droplet drag force	Dynamic drag model [40]
Droplet collision	NTC model [38]
Droplet coalescence	Post-collision outcome model [39]
Droplet turbulent dispersion	O'Rourke model [41]
Droplet evaporation	Frossling correlation-based model [42]

Table 4 Modeling parameters

KH model constants	$B_0 = 0.61, B_1 = 10$
RT model constants	$C_{RT} = 0.1$, $C_\tau = 1$
RANS constants	$C_\mu = 0.0845$, $C_{\epsilon 1} = 1.42$, $C_{\epsilon 2} = 1.68$, $C_{\epsilon 3} = -1.0$
Initial turbulent kinetic energy (TKE)	$k_0 = 1\,\mathrm{m}^2/\mathrm{s}^2$
Initial TKE dissipation rate	$\varepsilon_0 = 90\,\mathrm{m}^2/\mathrm{s}^3$
Cone angle	20 deg
Discharge coefficient	$C_d = 0.86$
N-dodecane mass diffusivity constants	$D_0 = 4.16 \cdot 10^{-6}$, $n_0 = 1.6$
Methanol mass diffusivity constants	$D_0 = 1.336 \cdot 10^{-5}$, $n_0 = 1.8$

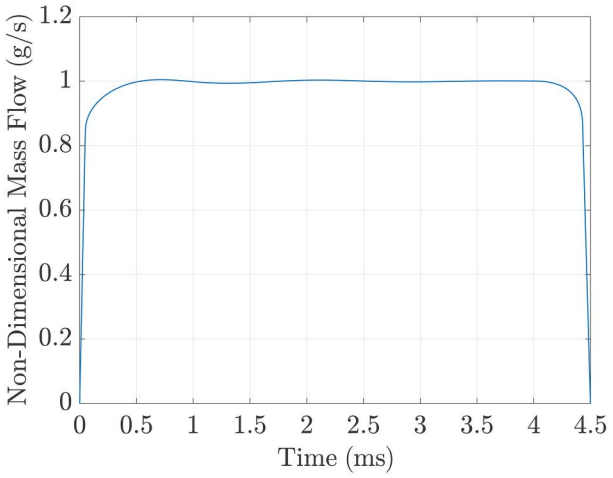

Fig. 3 Spray D rate of injection (ROI) profile for 150 MPa injection pressure (provided by Ref. [43])

3.3 Numerical Setup. The details of the used model parameters are presented in Table 4. These modeling parameters were kept constant for both n-dodecane and methanol injection cases. To calculate the liquid and vapor penetration, a 95% threshold for the liquid mass fraction and a threshold of 0.1% of fuel vapor mass fraction was used, respectively. The rate-of-injection (ROI) profile was defined according to the measurements provided by ECN for the 150 MPa injection pressure case [43]. Moreover, Fig. 3 depicts the normalized nondimensional mass flow ROI profile that was used in the present study.

4 Results and Discussion

In this section, we present the validation of our numerical model using the publicly available ECN Spray D data. Consequently, we convert our model for methanol operation and conduct an explicit comparison with the n-dodecane spray model. Since methanol exhibits nearly half the lower heating value (LHV) of diesel, three extra models were run using increased injection quantities to account for equal energy content with diesel. By keeping the injection duration constant, these models utilized three different nozzle diameters to achieve the increased methanol quantity, which account for 100, 150, and 200 MPa injection pressure. Lastly, for the 150 MPa injection pressure simulation case, we investigated the effect of initial ambient temperature and evaluated the cooling effect.

4.1 Model Validation. We used the liquid and vapor penetration experimental data provided by ECN to validate our CFD setup. In Fig. 4, we compare the simulated liquid and vapor penetration with the experimental results. The model captures the liquid length accurately, while the vapor penetration is slightly overpredicted due to the employed mesh size.

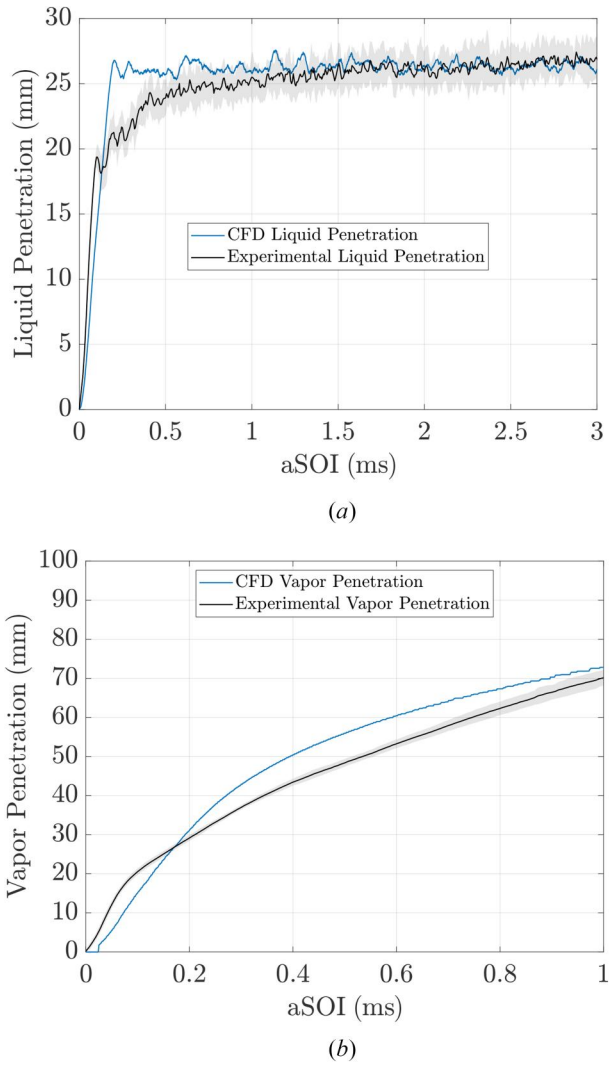

Fig. 4 Validation for liquid and vapor penetration predictions for the diesel baseline model showing both CFD and ECN Spray D experimental results: (*a*) liquid penetration and (*b*) vapor penetration

Moreover, Fig. 5 depicts the spatial comparison of the spray morphology between the experiment and the simulation. For the comparison, we used the mass fraction contours along with the Lagrangian particles to demonstrate the predictive capabilities of the presented model. The CFD spray morphology also reflects the slight overprediction in the vapor penetration. Despite the inability of the model to predict the initial flow dynamics, the predicted final liquid and vapor penetrations are within and near the experimental uncertainties presented in Fig. 4 as a gray shaded area. Based on the presented results, we consider the model validated for the scope of our study. Thus, the presented n-dodecane spray model is employed as the baseline model for the following methanol spray calculations.

4.2 Spray D Style Methanol Injection. Initially, we conducted an explicit comparison between the baseline diesel model and methanol. Figure 6 compares the liquid and vapor penetration of the two fuels using the same injection quantity. Methanol exhibits slightly lower liquid length and similar vapor penetration compared to diesel. These outcomes align with the study of Wang et al. [21], which investigated light-duty CI engine conditions. Methanol injection facilitates increased evaporation rates originating from its lower boiling point. Hence, the model successfully captured the decreased liquid length under the designated HD conditions.

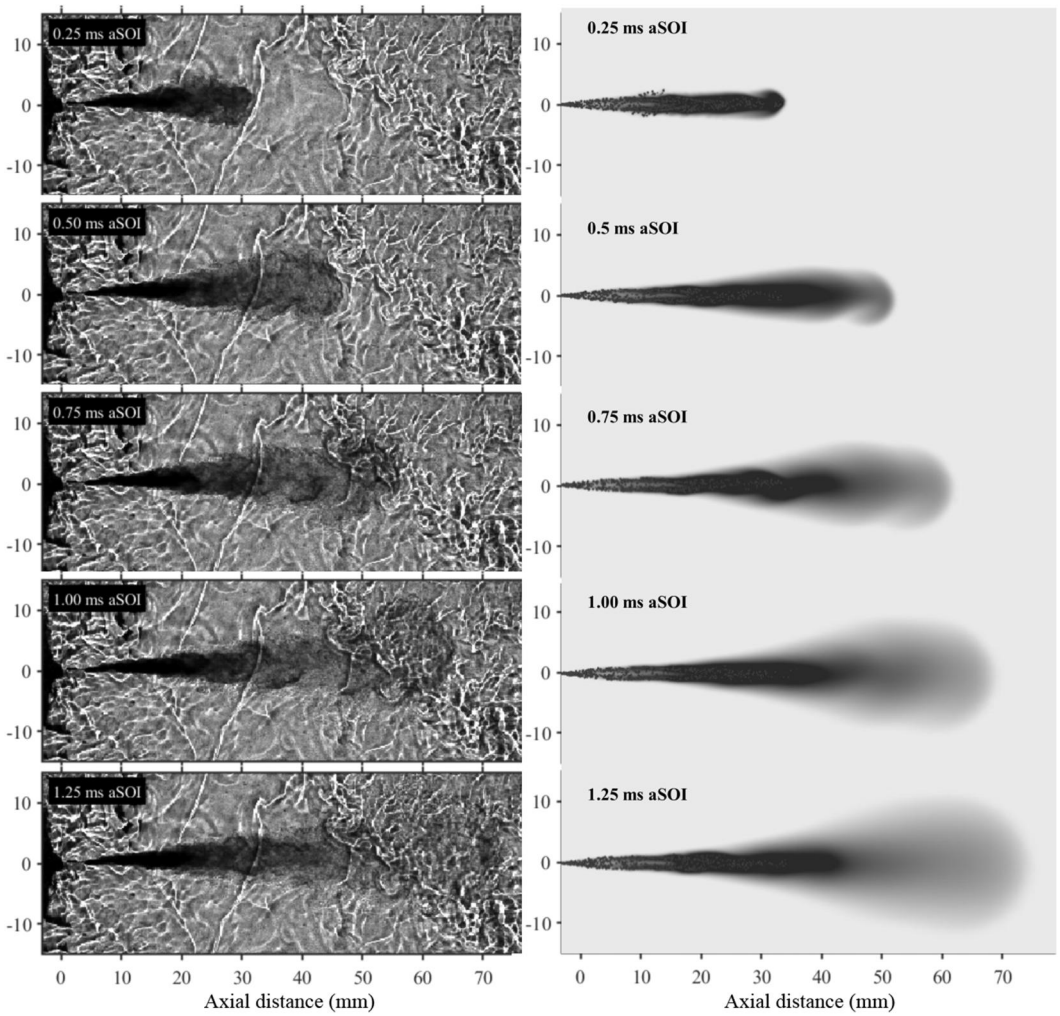

Fig. 5 Comparison of spray morphology of ECN Spray D (left) and CFD n-dodecane mass fraction (right). Experimental results provided to ECN by Sandia National Laboratories [26,44].

The increased evaporation of methanol is also observed in the fuel mass fraction contours (Fig. 7). Methanol's spray structure is similar to diesel's, but slightly increased mass fractions of evaporated fuel are observed in the vicinity of the spray. Furthermore, Fig. 8 depicts the mixture temperature during the initial stage of the injection. Due to intense evaporation conditions, the mixture cooling effect is observed in the plotted contours by the low temperature in the vicinity of the spray.

Thus, methanol exhibits reduced temperature zones under 630 K, while temperature at the same location in the diesel simulation is higher than 660 K. However, this difference may also be influenced partially by methanol's slightly increased evaporation rate.

4.3 Equal-Energy Methanol Injection. To accommodate equal energy injection quantities, we run three cases with increased fuel mass flow rates accounting for 100, 150, and 200 MPa injection pressure, and altered nozzle diameter. The injection duration was maintained constant by altering the nozzle diameter to accommodate the required mass flowrate for the designated injection pressure. The aim was to maintain the injection pressure at a predefined value to achieve similar initial bulk velocity of the spray jet as the initial simulation cases. Thus, by keeping the velocity of the jet similar, the effect of evaporation cooling due to methanol's properties could be isolated. Thus, the nozzle diameter for each case is the following:

- For 100 MPa injection pressure, $D_{noz} = 0.298$ mm.
- For 150 MPa injection pressure, $D_{noz} = 0.269$ mm.
- For 200 MPa injection pressure, $D_{noz} = 0.25$ mm.

Figure 9 presents the liquid and vapor penetrations for the equal energy models and the baseline diesel and methanol cases.

Particularly in the lower injection pressure case of the equal energy methanol injection, the liquid length is substantially increased. This is justified by the lower injection pressure case, which produces larger droplets due to increased nozzle diameter, which evaporate at a decreased rate. Moreover, the low injection pressure sprays have a decreased tendency for droplet breakup due to decreased jet velocity. This tendency is reflected by the spray Sauter Mean Diameter for the initial stages of the injection (Fig. 10). Similar trends are also observed for the vapor penetration of the equal energy methanol cases. Contrary to the results for the liquid length, the higher injection pressure cases produced slightly higher vapor penetration lengths. Figure 11 presents the mixture temperature for the equal energy methanol injection cases. For the increased injection quantities, the mixture temperature contours display enlarged cooled zones with temperatures lower than 600 K. These zones may impact significantly the combustion by forming zones of cooled mixture, which hinder the flame propagation phenomena.

In the case of methanol premixing, increased methanol substitution may induce increased cycle-to-cycle variability and unstable operation. A quantitative comparison of the mixture cooling in the vicinity of the spray is plotted in Fig. 12. For the equal energy cases, the temperature drop in the vicinity of the spray (40 mm axial location downstream) can reach up to 340 K. This decrease is significantly more intense than the diesel baseline case,

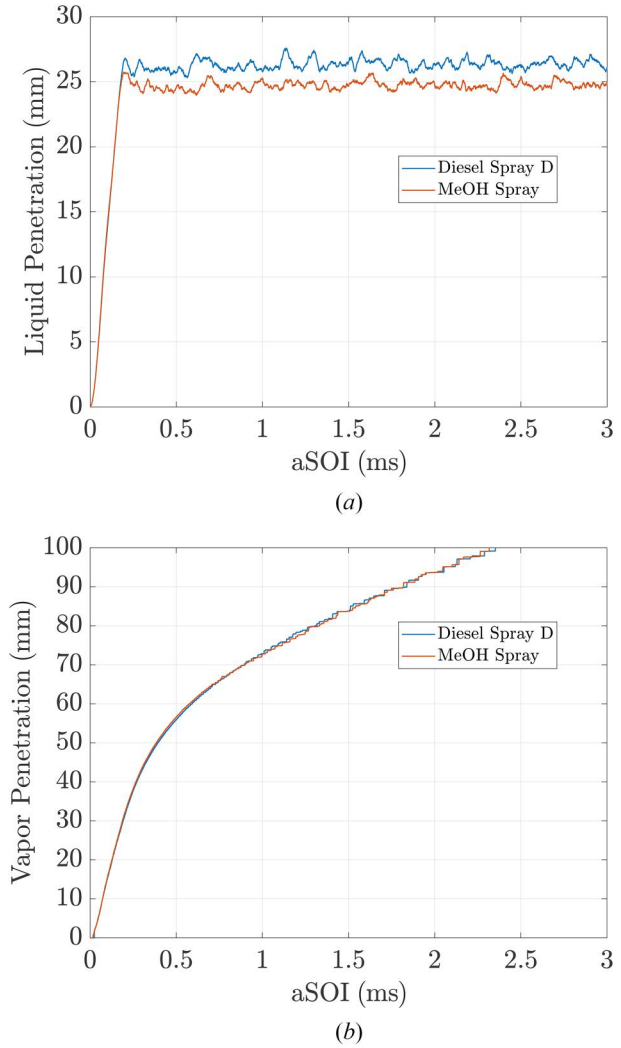

Fig. 6 Comparison of liquid and vapor penetration between diesel and methanol using equal injection quantity: (*a*) liquid penetration and (*b*) vapor penetration

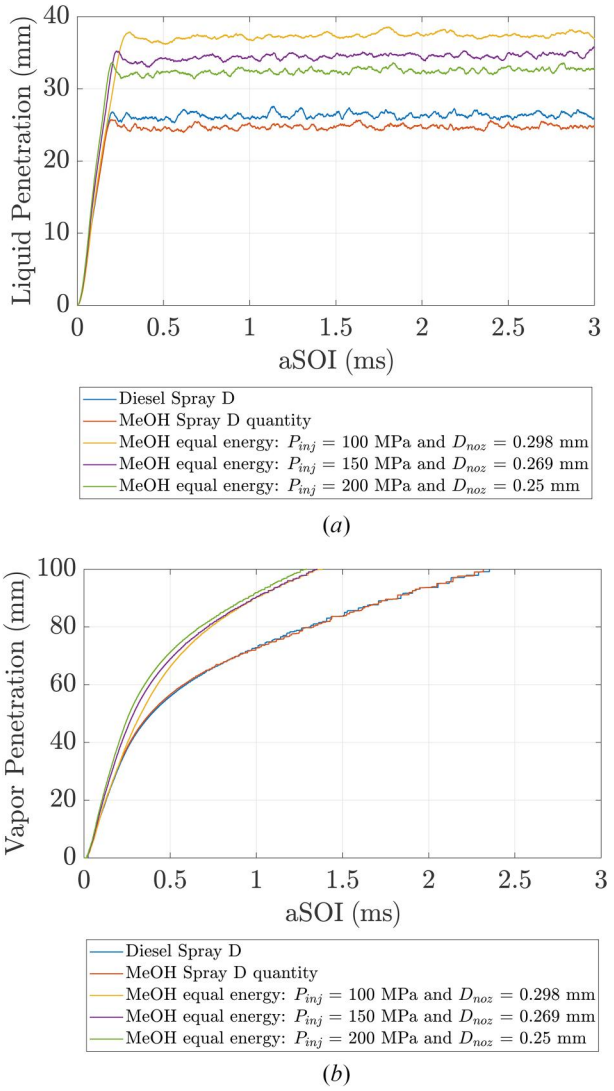

Fig. 9 Comparison of liquid and vapor penetration between diesel and methanol using equal quantity and equal energy injections: (*a*) liquid penetration and (*b*) vapor penetration

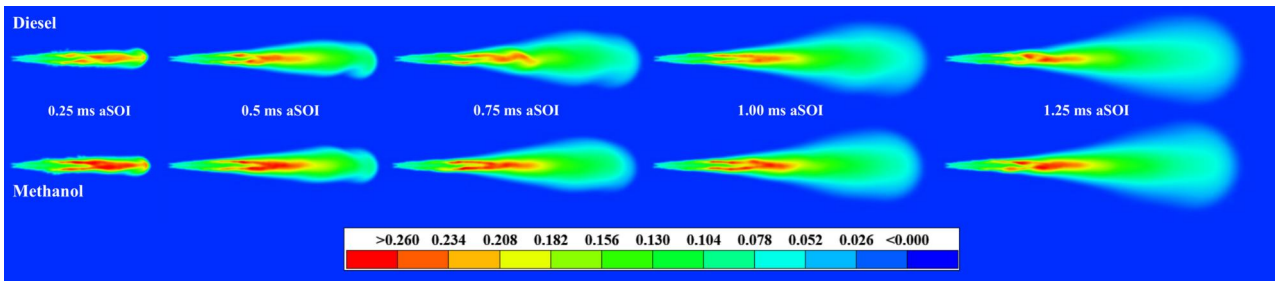

Fig. 7 Mass fraction contours comparison between diesel Spray D baseline model and methanol for equal quantity injection

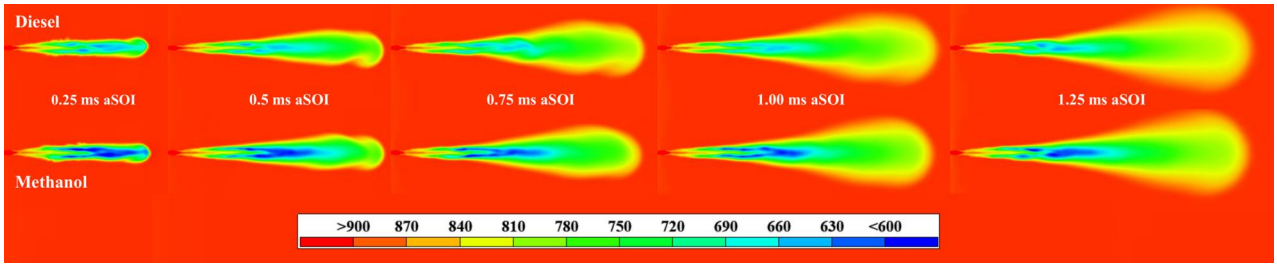

Fig. 8 Mixture temperature for equal quantity diesel and methanol injection

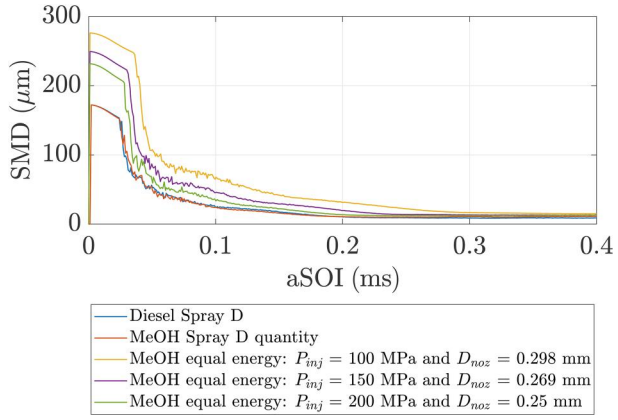

Fig. 10 Comparison of Spray SMD between diesel and methanol using equal quantity and equal energy injections

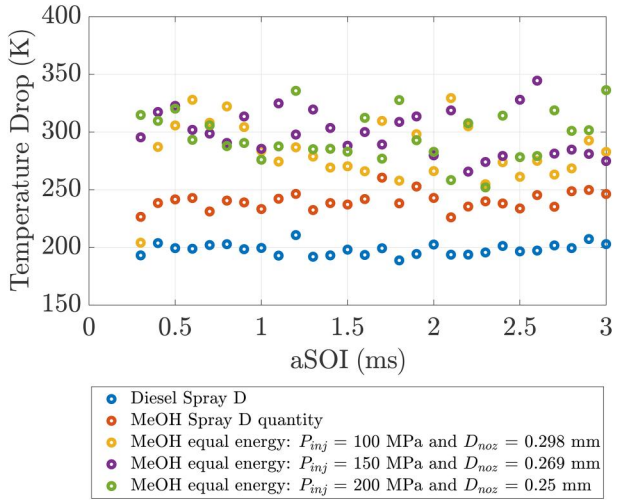

Fig. 12 Temperature drop at $z = 40$ mm axial location downstream

with an average temperature drop of 200 K. Lastly, Table 5 shows the average temperature drop in the vicinity of the spray. In the equal energy cases, the different injection pressures lead to similar mixture cooling intensity, while diesel has a much less intense cooling effect exhibiting up to 100 K increased mixture temperature.

4.4 Cooling Effect Sensitivity - Ambient Temperature Variation. In this section, we studied the mixture cooling under altered initial ambient temperatures using the equal energy methanol case with 150 MPa injection pressure. The tested range included ambient temperatures of 500, 700, 900, and 1100 K, while all the other parameters were kept constant. Here, the aim is to provide preliminary insights on varying methanol injection timings, which correspond to different levels of mixing ranging from premixed injection, during compression, to nonpremixed injection near TDC. Figure 13 illustrates the temperature contours for each reported ambient temperature case. Due to varying scales of mixture temperature, the color bar was varied accordingly to accommodate the initial assigned ambient temperature as the maximum value. For the higher initial ambient temperature cases, the cooling zones are significantly increased demonstrating a very intense cooling effect. The cooling intensity increases progressively and in proportion with the increase of initial ambient temperature.

Figure 14 illustrates the temperature difference between the initial ambient temperature of each case and the point, which is 40 mm downstream in the axial direction. In the high ambient temperature cases (i.e., 900 and 1100 K), the rapid evaporation rate causes a significant temperature drop of 299.4 K and 351.3 K, respectively (Table 6). However, these cases are related to near-TDC late injection conditions, when the piston has reached TDC.

Table 5 Average temperature drop at $z = 40$ mm axial location downstream

Case	Average temperature drop (K)
Diesel Spray D	198.3
Methanol Spray D quantity	240.2
Methanol equal energy: $P_{inj} = 100$ MPa and $D_{noz} = 0.298$ mm	283.1
Methanol equal energy: $P_{inj} = 150$ MPa and $D_{noz} = 0.269$ mm	299.4
Methanol equal energy: $P_{inj} = 200$ MPa and $D_{noz} = 0.25$ mm	297.0

Considering compression to be an approximately adiabatic process [45], then the cooled zones in the cylinder prior to combustion will be enlarged. Thus, after the mixture formation is completed, these cooled zones will inevitably act as an impediment to flame propagation and stable combustion. As a result, in early-like injection conditions, the mixture cooling is more impactful in the lower ambient temperature case (500 K), where the average temperature drop is around 100 K.

5 Conclusions

In this paper, we analyzed the implications of methanol DI sprays on the mixture temperature in the context of HD-DF engines. The

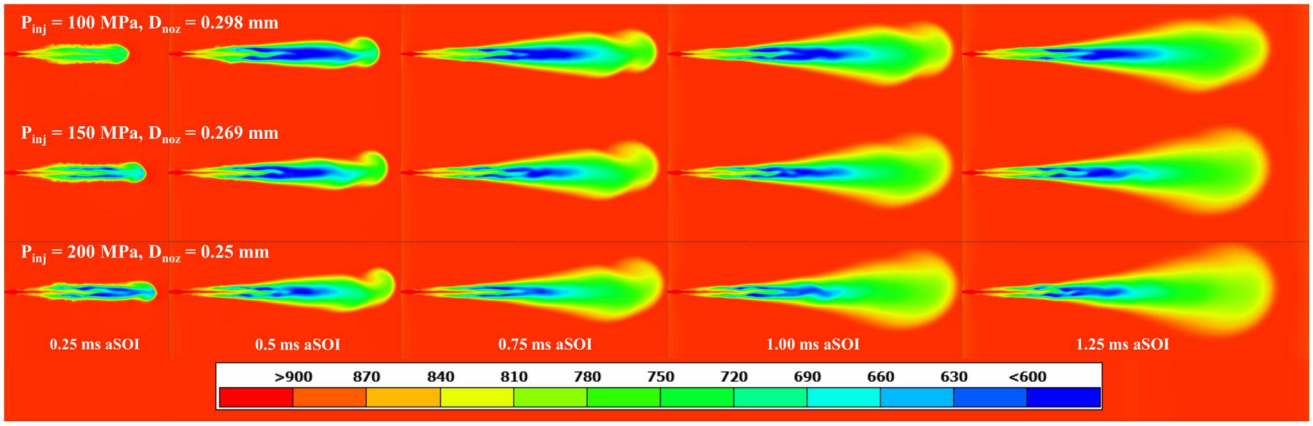

Fig. 11 Mixture temperature for equal energy methanol injection for 100, 150, and 200 MPa injection pressure

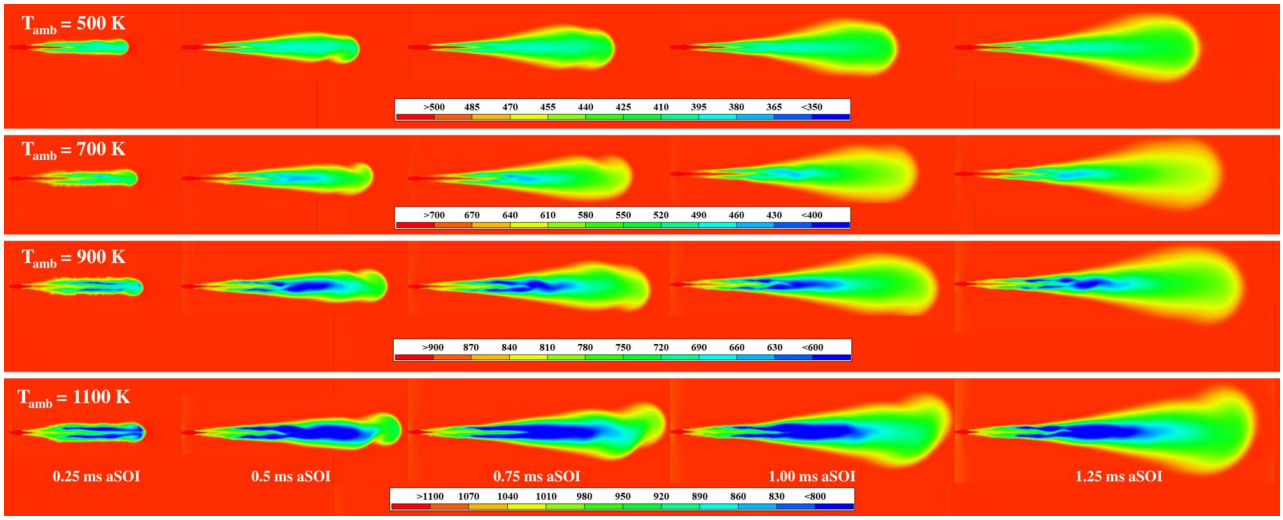

Fig. 13 Mixture temperature for different ambient temperatures

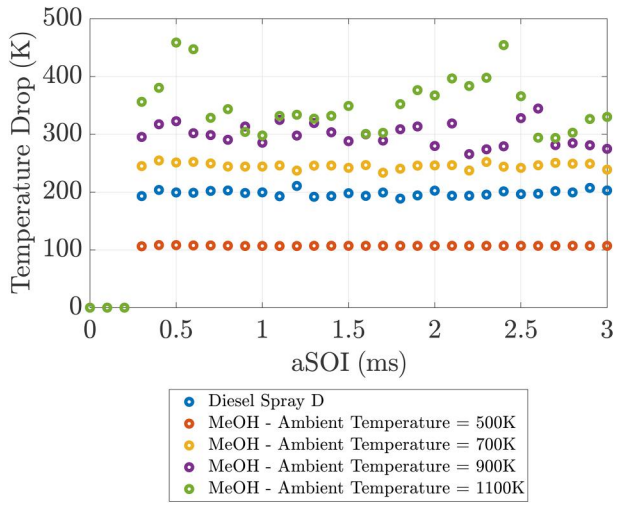

Fig. 14 Temperature drop for 150 MPa equal energy methanol injection under different initial ambient temperatures at $z = 40$ mm axial location downstream

Table 6 Ambient temperature variation: average temperature drop at $z = 40$ mm axial location downstream

Case	Average temperature drop (K)
Diesel Spray D	198.3
Methanol - ambient temperature = 500 K	107.1
Methanol - ambient temperature = 700 K	245.4
Methanol - ambient temperature = 900 K	299.4
Methanol - ambient temperature = 1100 K	351.3

simulated conditions were characterized by a high ambient pressure and temperature environment, which resembles DICI near-TDC and, in the lower ambient temperature cases, early-stroke injection conditions. The presented approach used ECN nonreacting Spray D data with diesel as the baseline case to validate the CFD spray model. The validated model was then converted for methanol injection under equal quantity and equal energy content as the diesel baseline. Consequently, using the equal energy model, we performed a sensitivity analysis on the ambient temperature. By altering the initial temperature, we aimed to roughly recreate varying mixing levels during the compression stroke. The performance of each methanol model was compared with diesel based on the outcome mixture temperature and spray characteristics.

Our findings revealed a significant increase in the cooling intensity of methanol-air mixture formation, an effect mainly attributed to methanol's high latent heat of vaporization. Considering also methanol's decreased LHV, the average mixture temperature was significantly lower for injections under equal energy content as diesel. Specifically, our analysis demonstrated a drop in mixture temperatures of up to 300 K in the core of the spray plume, which was more than 100 K of temperature drop compared to diesel. Moreover, when methanol quantity was increased to facility equal energy injection as diesel, the liquid length was substantially increased due to slower evaporation rate, which could pose challenges with piston wall wetting. The mixture cooling was more pronounced for higher initial ambient temperatures due to rapid methanol evaporation. However, lower initial temperatures exhibited excessive mixture cooling of more than 100 K forming low temperature zones. These zones will eventually spread out in the cylinder in an uncertain way, and serve as the main cause of unstable combustion.

In conclusion, this study contributed an assessment of the charge cooling effect of methanol injection in DICI engines. By analyzing the spray and initial mixture formation prior to ignition, the impact of methanol's increased latent heat of vaporization on engines can be estimated. Future work could potentially apply the presented methodology and study the mixture formation in a full engine cylinder model. Thus, a link between the mixture formation and combustion with the methanol cooling effect can be established. Resolving the flow phenomena during the compression stroke prior to ignition is essential to improving methanol substitution while maintaining stable operation. In addition, potential measures to counteract the cooling effect could include the increase of air intake temperature and split injection of methanol. Furthermore, future methanol CFD models should incorporate methanol-dedicated spray experiments for proper validation. This step will ensure the accurate representation of the complex physics encompassing droplet breakup, evaporation, and mixing of methanol. This study's outcomes could provide a road-map to investigate further and implement advanced methanol-diesel CI combustion modes, which can ultimately reduce the emissions and carbon footprint of HD and marine engines.

Acknowledgment

The present research is part of the MENENS project (Methanol als Energiestap Naar Emissieloze Nederlandse Scheepvaart).

We would like to thank Convergent Science [23], and BETA CAE Systems [46] for offering their software (CONVERGE, ANSA & META) and their technical support for the accomplishment of this research. ANSA was used for geometry creation and preprocessing of the CFD model, CONVERGE for the CFD simulations, and META for postprocessing and visualization of the results. All simulations were run in parallel on the DelftBlue supercomputer [47].

Funding Data

- Netherlands Enterprise Agency (RVO: Rijksdienst voor Ondernemend Nederland) (Grant No. MOB21012; Funder ID: 10.13039/100013405).

Data Availability Statement

The datasets generated and supporting the findings of this article are obtainable from the corresponding author upon reasonable request.

Nomenclature

aSOI = after start of injection
CFD = computational fluid dynamics
DF = dual-fuel
DICI = direct injection compression ignition
ECN = engine combustion network
HD = heavy-duty
ICE = internal combustion engine
LES = large eddy simulation
PFI = port fuel injection
RANS = Reynolds averaged Navier Stokes
TDC = top dead center

References

[1] Kessel, D. G., 2000, "Global Warming—Facts, Assessment, Countermeasures," J. Pet. Sci. Eng., **26**(1–4), pp. 157–168.
[2] IMO, 2020, "International Maritime Organization: Fourth Greenhouse Gas Study 2020," International Maritime Organization, London, UK, accessed Feb. 5, 2023, https://www.imo.org/en/OurWork/Environment/Pages/Fourth-IMO-Greenhouse-Gas-Study-2020.aspx
[3] Maes, N., Dam, N., Somers, B., Lucchini, T., D'Errico, G., and Hardy, G., 2018, "Heavy-Duty Diesel Engine Spray Combustion Processes: Experiments and Numerical Simulations," SAE Paper No. 2018.
[4] Reitz, R. D., Ogawa, H., Payri, R., Fansler, T., Kokjohn, S., Moriyoshi, Y., Agarwal, A. K., et al., 2020, "IJER Editorial: The Future of the Internal Combustion Engine," Int. J. Engine Res., **21**(1), pp. 3–10.
[5] Kalghatgi, G., 2018, "Is It Really the End of Internal Combustion Engines and Petroleum in Transport?," Appl. Energy, **225**, pp. 965–974.
[6] Tuner, M., 2016, "Review and Benchmarking of Alternative Fuels in Conventional and Advanced Engine Concepts With Emphasis on Efficiency, CO_2, and Regulated Emissions," SAE Paper No. 2016-01-0882.
[7] Ait Allal, A., Mansouri, K., Youssfi, M., and Qbadou, M., 2019, "Toward an Evaluation of Marine Fuels for a Clean and Efficient Autonomous Ship Propulsion Energy," Mater. Today: Proc., **13**, pp. 486–495.
[8] Verhelst, S., Turner, J. W., Sileghem, L., and Vancoillie, J., 2019, "Methanol as a Fuel for Internal Combustion Engines," Prog. Energy Combust. Sci., **70**, pp. 43–88.
[9] Pipicelli, M., Di Luca, G., Ianniello, R., Gimelli, A., and Beatrice, C., 2022, "Alcohol Fuels in Compression Ignition Engines," Energy, Environment, and Sustainability, Springer, Singapore, pp. 9–31.
[10] Zincir, B., and Deniz, C., 2021, "Methanol as a Fuel for Marine Diesel Engines," Energy, Environment, and Sustainability, Springer, Singapore, pp. 45–85.
[11] Korberg, A. D., Brynolf, S., Grahn, M., and Skov, I. R., 2021, "Techno-Economic Assessment of Advanced Fuels and Propulsion Systems in Future Fossil-Free Ships," Renewable Sustainable Energy Rev., **142**, p. 110861.
[12] Karim, G. A., 2015, *Dual-Fuel Diesel Engines*, CRC Press, Boca Raton, FL.
[13] Krishnasamy, A., Gupta, S. K., and Reitz, R. D., 2021, "Prospective Fuels for Diesel Low Temperature Combustion Engine Applications: A Critical Review," Int. J. Engine Res., **22**(7), pp. 2071–2106.
[14] Karimkashi, S., Gadalla, M., Kannan, J., Tekgül, B., Kaario, O., and Vuorinen, V., 2023, "Large-Eddy Simulation of Diesel Pilot Spray Ignition in Lean Methane-Air and Methanol-Air Mixtures at Different Ambient Temperatures," Int. J. Engine Res., **24**(3), pp. 965–981.
[15] Shamun, S., Zincir, B., Shukla, P., Garcia Valladolid, P., Verhelst, S., and Tunér, M., 2018, "Quantification and Analysis of the Charge Cooling Effect of Methanol in a Compression Ignition Engine Utilizing PPC Strategy," ASME Paper No. ICEF2018-9657.
[16] Svensson, M., Tuner, M., and Verhelst, S., 2022, "Low Load Ignitability of Methanol in a Heavy-Duty Compression Ignition Engine," SAE Paper No. 2022-01-1093.
[17] Zincir, B., Shukla, P., Shamun, S., Tuner, M., Deniz, C., and Johansson, B., 2019, "Investigation of Effects of Intake Temperature on Low Load Limitations of Methanol Partially Premixed Combustion," Energy Fuels, **33**(6), pp. 5695–5709.
[18] Dong, Y., Kaario, O., Hassan, G., Ranta, O., Larmi, M., and Johansson, B., 2020, "High-Pressure Direct Injection of Methanol and Pilot Diesel: A Non-Premixed Dual-Fuel Engine Concept," Fuel, **277**, p. 117932.
[19] Matamis, A., Lonn, S., Luise, L., Vaglieco, B. M., Tuner, M., Andersson, O., Alden, M., and Richter, M., 2021, "Optical Characterization of Methanol Compression-Ignition Combustion in a Heavy-Duty Engine," Proc. Combust. Inst., **38**(4), pp. 5509–5517.
[20] Dierickx, J., Verbiest, J., Janvier, T., Peeters, J., Sileghem, L., and Verhelst, S., 2021, "Retrofitting a High-Speed Marine Engine to Dual-Fuel Methanol-Diesel Operation: A Comparison of Multiple and Single Point Methanol Port Injection," Fuel Commun., **7**, p. 100010.
[21] Wang, Y., Dong, P., Long, W., Tian, J., Wei, F., Wang, Q., Cui, Z., and Li, B., 2022, "Characteristics of Evaporating Spray for Direct Injection Methanol Engine: Comparison Between Methanol and Diesel Spray," Processes, **10**(6), p. 1132.
[22] Kaario, O. T., Karimkashi, S., Bhattacharya, A., Vuorinen, V., Larmi, M., and Bai, X., 2024, "A Comparative Study on Methanol and n-Dodecane Spray Flames Using Large-Eddy Simulation," Combust. Flame, **260**, p. 113277.
[23] CONVERGE, 2024, "CONVERGE CFD Software Website," CONVERGE, Northville, MI, accessed Nov. 13, 2024, https://convergecfd.com/
[24] Agarwal, A. K., Gautam, A., Sharma, N., and Singh, A. P., 2019, *Methanol and the Alternate Fuel Economy*, Springer, Singapore.
[25] Zoumpourlos, K., Coraddu, A., Geertsma, R., and van de Ketterij, R., 2023, "Evaluation of Methanol Sprays in Marine Internal Combustion Engines: A Case Study for Port Fuel Injection Systems," Proceeding of Modelling and Optimisation of Ship Energy Systems Conference, Delft, The Netherlands, Oct. 26–27.
[26] ECN, 2024, "Engine Combustion Network Spray-D Nozzle Geometry," ECN, Wellington, New Zealand, accessed Sept. 1, 2023, https://ecn.sandia.gov/diesel-spray-combustion/target-condition/spray-d-nozzle-geometry/
[27] ECN, 2023, "Engine Combustion Network Spray-M Data," ECN, Wellington, New Zealand, accessed Oct. 7, 2023, https://ecn.sandia.gov/data/sandia-spray-m-data/
[28] Senecal, P., Pomraning, E., Richards, K., and Som, S., 2012, "Grid-Convergent Spray Models for Internal Combustion Engine CFD Simulations," ASME Paper No. JERT-13-1108.
[29] Han, Z., and Reitz, R. D., 1995, "Turbulence Modeling of Internal Combustion Engines Using RNG κ-ε Models," Combust. Sci. Technol., **106**(4–6), pp. 267–295.
[30] CONVERGE CFD Software, 2022, *CONVERGE MANUAL v3.0*, Convergent Science Inc., Madison, WI.
[31] Issa, R. I., 1986, "Solution of the Implicitly Discretised Fluid Flow Equations by Operator-Splitting," J. Comput. Phys., **62**(1), pp. 40–65.
[32] Ferziger, J. H., Perić, M., and Street, R. L., 2002, *Computational Methods for Fluid Dynamics*, Vol. 3, Springer Nature, Switzerland.
[33] Horvath, A., 1974, "Redlich-Kwong Equation of State: Review for Chemical Engineering Calculations," Chem. Eng. Sci., **29**(5), pp. 1334–1340.
[34] Di Matteo, A., Bao, H., and Somers, B., 2022, "Modeling Spray C and Spray D With FGM Within the Framework of RANS and LES," Front. Mech. Eng., **8**, p. 1013138.
[35] Kalwar, A., Chintagunti, S., and Agarwal, A. K., 2021, "Gasohol Sprays Simulations of a Multi-Hole GDI Injector in Engine-Like Conditions," SAE Paper No. 2021-01-0549.
[36] Reitz, R. D., and Diwakar, R., 1987, "Structure of High-Pressure Fuel Sprays," SAE Trans., pp. 492–509.
[37] Beale, J. C., and Reitz, R. D., 1999, "Modeling Spray Atomization With the Kelvin-Helmholtz/Rayleigh-Taylor Hybrid Model," Atomization Sprays, **9**(6), pp. 623–650.
[38] Schmidt, D. P., and Rutland, C. J., 2000, "A New Droplet Collision Algorithm," J. Comput. Phys., **164**(1), pp. 62–80.
[39] Post, S. L., and Abraham, J., 2002, "Modeling the Outcome of Drop–Drop Collisions in Diesel Sprays," Int. J. Multiphase Flow, **28**(6), pp. 997–1019.
[40] Liu, A. B., Mather, D., and Reitz, R. D., 1993, "Modeling the Effects of Drop Drag and Breakup on Fuel Sprays," SAE Trans., pp. 83–95.
[41] O'Rourke, P. J., 1989, "Statistical Properties and Numerical Implementation of a Model for Droplet Dispersion in a Turbulent Gas," J. Comput. Phys., **83**(2), pp. 345–360.
[42] Miller, R., Harstad, K., and Bellan, J., 1998, "Evaluation of Equilibrium and Non-Equilibrium Evaporation Models for Many-Droplet Gas-Liquid Flow Simulations," Int. Journal Multiphase Flow, **24**(6), pp. 1025–1055.
[43] CMT, 2016, "Spray C/D Rate of Injection," Clean Mobility and Thermofluids, Valencia, Spain, accessed Sept. 1, 2023, https://www.cmt.upv.es/#/ecn/download/nozzlecharac/ncSprayCDRateOfInj
[44] Maes, N., Skeen, S. A., Bardi, M., Fitzgerald, R. P., Malbec, L., Bruneaux, G., Pickett, L. M., Yasutomi, K., and Martin, G., 2020, "Spray Penetration, Combustion, and Soot Formation Characteristics of the ECN Spray C and Spray D Injectors in Multiple Combustion Facilities," Appl. Therm. Eng., **172**, p. 115136.
[45] Heywood, J. B., 2018, *Internal Combustion Engine Fundamentals*, McGraw-Hill Education, New York.
[46] cadence, 2024, "BETA CAE Systems Website," BETA CAE Systems International AG, Switzerland, accessed Nov. 13, 2023, https://www.beta-cae.com/
[47] Delft High Performance Computing Centre (DHPC), 2022, "DelftBlue Supercomputer (Phase 1)," Delft High Performance Computing Centre, CD Delft, The Netherlands, accessed July 11, 2022, https://www.tudelft.nl/dhpc/ark/delftbluephase1